Automotive Radar Signal and Interference Simulation for Testing Autonomous Driving

Alexander Prinz[1(✉)], Leo-Tassilo Peters[1], Johannes Schwendner[2], Mohamed Ayeb[3], and Ludwig Brabetz[3]

[1] Bayerische Motoren Werke AG, Petuelring 130, Munich, Germany
{alexander.prinz,leo-tassilo.peters}@bmw.de
[2] Expleo Germany GmbH, Munich, Germany
johannes.schwendner@expleogroup.com
[3] Universität Kassel, Wilhelmshöher Allee 73, 34121 Kassel, Germany
{ayeb,brabetz}@uni-kassel.de

Abstract. With the development of automated driving functions, more and more environmental sensors are combined for the vehicle perception. A problem that arises with the extensive use of radar sensing is called interference. It describes the confounding effects from the wave overlay of two or more radar sensors operating in the same frequency-band. At this point, methods for interference avoidance and mitigation come to apply. For a valid design and development of such methods, real sensor measurements were required in the past. This publication instead proposes a novel sensor modelling technique that represents the interference mechanisms within the radar sensor signals. It is based on a full radar time signal simulation coupled with a broad range of influencing factors. The concept is validated by comparing the simulated signal processing steps to the real sensor measurement behavior. As a result, mitigation methods for the sensor fault behavior can be fully assessed within a simulation environment. The opportunity for applying new scenario data and a variable set of radar sensors underlines the importance of this approach in the development of future radar systems.

Keywords: Driver assistance · Automotive radar · Radar interference · Sensor modelling · Sensor model validation · Testing process

1 Introduction

Continuous development of active safety has had a decisive impact on the accident statistics in the past years. In particular the effectiveness of a lane change warning was analyzed by the association of German insurance companies over a time duration of five years. According to their statistics, the deployment of such

A. L. Martins et al. (Eds.): INTSYS 2020, LNICST 364, pp. 223–240, 2021.
https://doi.org/10.1007/978-3-030-71454-3_14

systems has the potential to prevented 3.582 accidents and 5.191 injured traffic participants annually [1]. For that reason, most modern cars are equipped with these systems to fulfill the EuroNCAP test requirements [2]. This trend in active safety also drives the current development for more advanced driving functions. Beside safety reasons, automated driving also creates a new business model for private transportation. Especially in urban areas innovative driver-less mobility solutions can prevent traffic jams and save the space for parking facilities in the city area [3]. This promising innovation requires sophisticated systems that are capable to interact with the traffic environment. For that reason the perception task is one key element of modern assistance systems. Among the variety of automotive sensors, radar is a common technology for environment perception. Radar sensors use an active measurement principle by sending and receiving electromagnetic waves. The reserved frequency band for the automotive application is between 77 GHz and 81 GHz [4]. Compared to other environmental sensors, radar sensing can directly measure the range, azimuth angle, and radial velocity of a target with the help of a single measurement in a short period of time [5]. Furthermore the radar signal processing is very resilient to bad weather conditions [6]. Beside these advantages the application of radar sensors is problematic due to the effect of mutual interference [7]. Radar-Interference summarizes the effects that emerge when two or more radar sensors are operating in the same frequency-band at the same time. Previous trends also promote a higher likelihood for interference because more and more cars are equipped with a rising number of up to ten radar sensors [6]. Interference mitigation methods exist, but their applicability for a variety of scenarios is still unproven [8–10]. This research paper addresses this problem by presenting a novel radar simulation for the application and test of radar interference methods. In contrast to other publications from [11–13] this approach has the main focus on a closely meshed modelling and validation process. The application of this simulation enables a trustworthy evaluation of radar performance metrics for a variety of possible interference scenarios. This supports the development of radar interference mitigation methods for future driver assistance systems.

2 Radar Basics

2.1 Measurement Principle and Signal Processing for FMCW Radar

The most common technique in automotive radars is the generation of Frequency-Modulated Continuous Wave (FMCW) signals. The main idea of this waveform is to send out frequency modulated signals in a short period of time and repeat this several times. These signal portions are also called chirps and will be received after being reflected by a target. As a next step, the time signal at the receiver antennas $x_{\mathrm{rx}}(t)$ will be directly mixed with the transmitted signal $x_{\mathrm{tx}}(t)$. This results in the signal $x_{\mathrm{m}}(t)$ which can be sampled in a lower frequency band, the so called baseband. For an interpretation of the sampled time signal, it is transformed into the frequency domain. After applying a

two-dimensional Fourier Transformation (FT), the signal processing results in a complex matrix [5]. Then, the range-velocity map (RV-map) separates targets in radial distance and velocity. Each cell inside this matrix contains the amplitude and the phase of the corresponding spatial frequency bin. By comparing the amplitude of each cell with the neighbouring cells, targets can be detected on the RV-map [14]. While targets are separated in range- and velocity-domain, the azimuth angle can be estimated based on a single bin in the RV-map. The main idea about the angle estimation is the simultaneous sampling along a horizontally distributed antenna array. The angle of incidence α corresponds to a different pathway over the antenna array. By evaluating the phase change $\delta\theta$ the angle of incidence can be calculated as described in [15].

2.2 Interference on FMCW Radars

At first, Hischke [16] conducted a study on radar interference in automotive applications. From his investigations the exposure time and the signal-power of the received interference signal determines the severity of the effect. Based on these fundamentals, Brooker [8] worked out a distinction for the interfering effects. In case that two chirps have the same slope and both are sent out within a short time delay (˜ns), the **synchronous interference** can be observed. In addition, he analyzed interference from different waveforms and their intersection points. This case is summarized in the so called **asynchronous interference** and is more likely to occur because automotive radar systems typically differ in their transmitted waveform. For the time span around the intersection point the mixer signal frequency changes linearly [7]. Furthermore, the slope of the changing frequency portions is depending on the slopes difference of both radar waveforms. Subsequently, the mixer signal will be filtered by a high- and low pass in time domain. This suppresses the out-of band frequencies that cannot be interpreted by the radar sensors signal processing. In the end, the interfering signal portions are spread on all range-frequencies and will raise the noise floor in the subsequent processing steps [8,17]. An increased noise floor has a direct impact on the target detection because radar signal processing uses the Signal-to-Noise Ratio (SNR) to detect targets on the range-velocity map.

Due to the fact that radar interference is a serious problem for object detection, various researchers have worked on this topic. A first group of publications looked at theoretical aspects [12,18]. Others focused on empirical measurements [7,17,19]. Beside that some publications addressed the integration of an interference model in an environment simulation [11,20]. For differentiation, the model approach from [11] is modelling interference in the radar baseband. Whereas [20] simplified approach is only calculating the Signal-to-Interference-Ratio (SIR) to estimate the SNR-drop for the received target hit point. Since both model approaches were not combined with real sensor measurements, their validation is still pending. Based on the existing work, a general radar and interference simulation with good applicability is still missing. This can be traced back to a high effort in the acquisition of measurement data with distinct interference influence. Apart from that, the validation has to be considered on various levels in

the signal processing chain. At this point, the paper presents a novel radar time signal simulation with all relevant interfaces for the applied validation strategy. The resulting simulation framework can be used for the test and development of interference mitigation techniques.

3 Automotive Radar Simulation

3.1 Architecture and Interfaces

The architecture of the automotive radar simulation is combining a virtual vehicle environment with a radar time signal simulation and its signal processing. Besides that, the architecture in Fig. 1 has to ensure that the different processing levels are clearly defined. This is particularly relevant for the bidirectional comparison in the validation procedure. The first layer in the simulation handles the scenario which describes the observed vehicles and their interaction in the driving situation. The scenario itself can be derived from the accident statistics in [1]. Based on the scenario data the geometric hit points can be generated from the parametrized sensor resolution on the second level. On the third level, the hit points of each time step in simulation will be converted into time signals. The superposition properties allow us to generate the signals from each hit point independently. Subsequently the sampling layer on the radar front-end accumulates the time-discrete signals. A signal processing model is then applied to compare the scenario input and simulation output hit points directly over the scenario. In the development of interference mitigation techniques, the hit point loss over the scenario time has to be minimized.

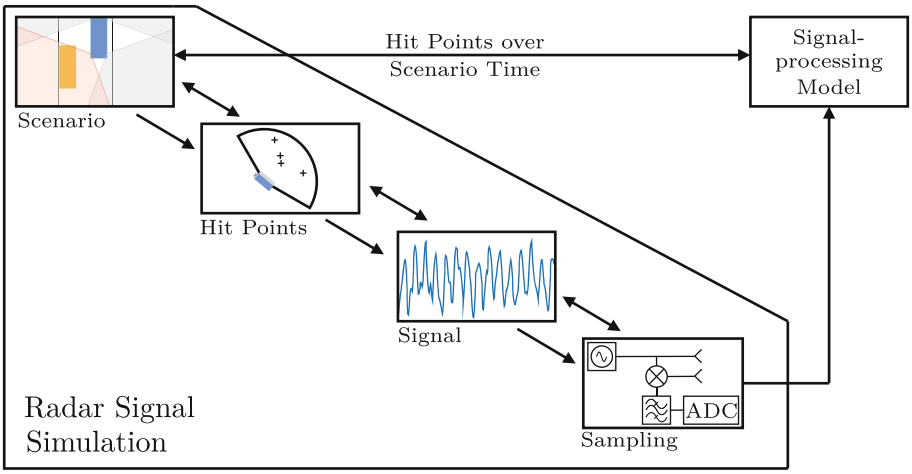

Fig. 1. General architecture and model interfaces: the simulation runs top-down (single arrows) while the validation is also applied bottom-up (double arrow).

3.2 Radar Signal Simulation

The scenario environment is capable of predicting the perception of the sensor based on a concrete driving scenario. For this reason, each traffic participant in the sensors Field-of-View (FoV) corresponds to a number of geometrical hit points. These reflection points can be described in radial distance r, radial velocity $\dot{r}$ and azimuth angle α based on the resolution of the sensor [21].

As a next step, the simulated geometrical hit points will be transferred into the *Hit Point Time Signal* block (see Fig. 2) which generates the echo time signal. For each antenna the target is interpreted as a sum of independent echos.

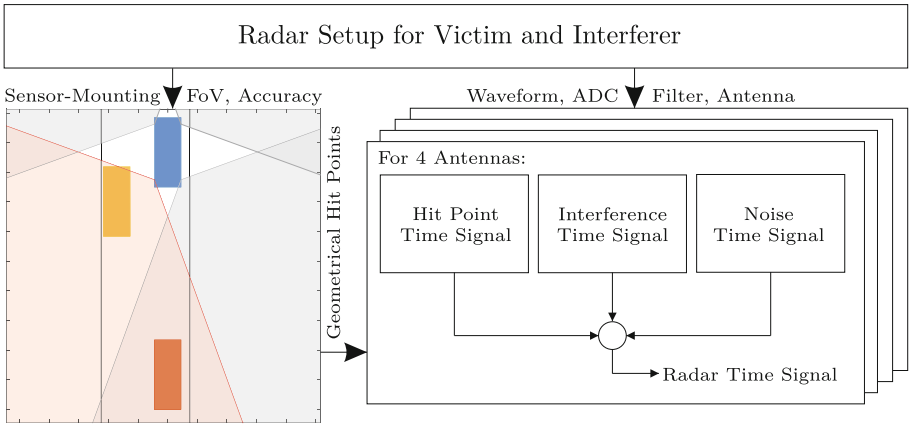

Fig. 2. Radar time signal calculation based on simulated hit points and interference. (Color figure online)

The *Interference Time Signal* block generates the received radar signal from an interferer. As part of the *Noise Time Signal* block, the noise in the radar front-end is synthetically generated. In the end, all three components get superimposed. The time signal equations will be analytically derived in the following.

Hit Point Time Signal. The Hit Point Time Signal is based on the general principle of the radar front-end illustrated in Fig. 3. First, the local oscillator (LO) is generating frequency modulated chirps in the radar band. Then, phase modulation (PSM) and power amplifier (PA) is applied and the Tx-antenna is emitting the radar transmit signal $x_{\mathrm{tx}}(t)$. After being reflected by the object, the received echo signal $x_{\mathrm{rx}}(t)$ is amplified by the low noise amplifier (LNA) and transferred into the baseband $x_{\mathrm{m}}(t)$. After that, the signal is filtered with a high-pass filter (HPF) and a variable gain amplifier (VGA) can be adjusted to prevent saturation. Finally, the low-pass filtered signal is sampled

by an analog-to-digital converter (ADC) and is ready for further digital signal processing.

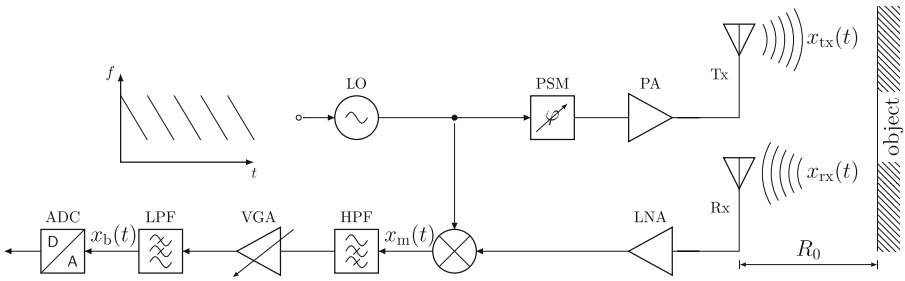

Fig. 3. Radar front-end is processing the time signal from a reflecting object.

In a first step, the frequency f can be defined as a function of time, where $f_{s,ref}$ is the start frequency. The chirp's slope $\mu = B/T_c$ leads to a linear function of the frequency over time.

$$f(t) = f_{s,ref} + \mu \cdot t \tag{1}$$

The phase over time can be written as the integral of the frequency of the signal.

$$\phi(t) = 2\pi \cdot \int f(t)dt = 2\pi f_{s,ref} t + \pi \mu t^2 + \phi_0 \tag{2}$$

This expression can be used to describe the transmitted signal amplitude $x_{tx}(t)$ by a trigonometric function.

$$x_{tx}(t) = A_{tx} cos(2\pi f_{s,ref} t + \pi \mu t^2 + \phi_0) \tag{3}$$

For the received signal amplitude $x_{rx}(t)$ the time variable t is substituted by $(t - \tau)$ where τ is the time delay between sending and receiving the signal. A_{tx} and A_{rx} describe the signal's amplitude and are linked to the receiver gain, pathloss and transmission power.

$$x_{rx}(t) = A_{rx} cos\big(2\pi f_{s,ref}(t-\tau) + \pi \mu (t-\tau)^2 + \phi_0\big) \tag{4}$$

The time signal of the mixer in Fig. 3 is derived by these two time signals

$$x_m(t) = x_{rx}(t) \cdot x_{tx}(t). \tag{5}$$

With the help of Euler's formula the signals can be transformed and the mixed signal $x_m(t)$ can be written as a function of sum and difference phase.

$$x_m(t) = \frac{A_{tx} \cdot A_{rx}}{2} \big(cos(\phi_{dif}(t)) + cos(\phi_{sum}(t))\big) \tag{6}$$

According to [22] the phase portions from $\phi_{\text{sum}}(t)$ result in an oscillation with a frequency greater than that originally sent. The latter will be eliminated by the low-pass-filter in Fig. 3 so only the $\phi_{\text{dif}}(t)$ has to be considered for the beat signal $x_{\text{b,tar}}(t)$ in Eq. 7.

$$x_{\text{b,tar}}(t) = \frac{A_{\text{tx}} \cdot A_{\text{rx}}}{2} \left(cos(2\pi f_{\text{s,ref}} \tau + 2\pi\mu\tau t - \pi\mu\tau^2) \right) \tag{7}$$

The trip time τ is related to the radial distance R_0 at the beginning t_0 of the chirp. The radial velocity v_r of the reflecting object is assumed to be constant during the chirp-duration T_c.

$$\tau(t) = 2 \cdot \frac{R_0 + v_r(t - t_0)}{c_0} \quad \text{with} \quad t \in [t_0, t_0 + T_c] \tag{8}$$

With the given trip time τ the beat signal can be derived by the hit point state variables in Eq. 9. Beside that, the quadratic τ-terms were neglected because they have no quantifiable impact on the beat signal $x_{\text{b,tar}}(t)$.

$$x_{\text{b,tar}}(t) = \frac{A_{\text{tx}} \cdot A_{\text{rx}}}{2} cos\Big(2\pi \Big(2 f_{\text{s,ref}} \frac{R_0}{c_0} + \underbrace{2 f_{\text{s,ref}} \frac{v_{\text{r}}}{c_0}}_{\text{Doppler}} t + \underbrace{2 R_0 \frac{\mu}{c_0}}_{\text{Range}} t \Big) \Big) \tag{9}$$

When analyzing Eq. 9, the Doppler frequency can be identified. In the simulation architecture from Fig. 1, the Eq. 9 is computed for every geometric hit point simulated in the environment simulation for all antenna positions. Then, the time signal of an extended object can be described by adding up the beat signals from the simulated point targets.

Interference Time Signal. Apart from the reflecting targets the simulated time signal also consists of mixing products from an interfering radar. The task of this simulation part is the analysis of the time signal of both radar waveforms. The following figure gives a better idea about the chirp superposition in frequency domain.

As shown in Fig. 4, a mixer signal is only present while both radars are transmitting. The current frequency-difference between reference- and interference-signal is changing over the time. The reason for this is the difference in chirp-slope of both radars. Beside the frequency-difference also the chirp time delay β for the interfering radar waveform has to be considered. Next, the simulation has to estimate the point in time $t_{\text{int,i}}$ where the interfering chirp i and the observed reference chirp have the same frequency according to Eq. 10.

$$t_{\text{int,i}} \cdot \mu_1 + f_{s,\text{ref}} = (t_{\text{int},i} - \beta) \cdot \mu_2 + f_{s,\text{int}} \quad \text{for} \quad t_{\text{int,i}} \in [t_{s,i}; t_{e,i}] \tag{10}$$

Based on this point in time, a time duration can be calculated for each of N_{int} interfering chirps. From Fig. 4 the chirp slope difference determines the derivative of the frequency deviation δf. For the considered application we recommend δf to be ten times higher than the low-pass frequency f_{LP}. With this given frequency

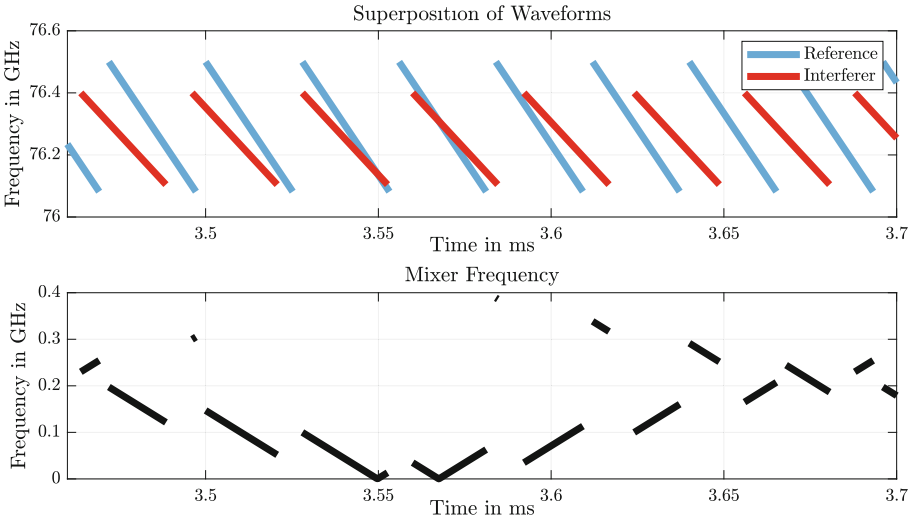

Fig. 4. The top plot visualizes the frequency over time of two radars operating in the same frequency band. In the lower plot the idealized mixer frequency is presented.

deviation δf, the interference time duration results in the time interval $[t_{s,i}; t_{e,i}]$ for each chirp number i. Then, the time bounded subsets can be unified to a superset M of all interfering time intervals.

$$M = \left\{ t \,|\, t_{s,i} < t < t_{e,i}, i \in \{1, \ldots N_{\text{int}}\} \right\} \tag{11}$$

After resolving the interference time interval M, the phase equations for both waveforms can similarly be formulated with reference to Eq. 2.

$$\phi_{\text{ref}}(t) = 2\pi \cdot \int f_{\text{ref}}(t)dt = 2\pi f_{s,\text{ref}} \cdot t + \pi\mu t^2 + \phi_{0,r} \tag{12}$$

$$\phi_{\text{int}}(t) = 2\pi \cdot \int f_{\text{int}}(t-\beta)dt = 2\pi f_{s,\text{int}} \cdot (t-\beta) + \pi\mu(t-\beta)^2 + \phi_{0,i} \tag{13}$$

As the transmit time signal in Eq. 3 persists, the corresponding receiver time signal can be estimated equally from the phase in Eq. 13. After applying the mixer from Eq. 5 and the Euler's formula in Eq. 6, the beat-signal from the interfering signal can be described as

$$x_{\text{b,int}}(t) = \frac{A_{\text{tx,ref}} A_{\text{tx,int}}}{2} \cdot \left(cos(\phi_{\text{dif,int}}(t)) \right) \tag{14}$$

with

$$\phi_{\text{dif,int}}(t) = 2\pi \Big(t^2 \Big(\frac{\mu_1 - \mu_2}{2} \Big) + t \Big(f_{\text{s,ref}} - f_{\text{s,int}} + \mu_2 \beta \Big) \ldots$$
$$\ldots - 0.5\mu_2\beta^2 + f_{\text{int},0}\beta \Big) + \phi_{0,\text{r}} - \phi_{0,\text{i}} \tag{15}$$

Now, the time portions from the interference time interval M can be inserted in Eq. 14 to finally get the active interference beat signal $x_{\mathrm{b,int}}(t)$. Due to the fact that the beat signal from a reflecting target is independent from the beat signal from an interfering radar the two signals can be added.

$$x_{\mathrm{b}}(t) = x_{\mathrm{b,tar}}(t) + x_{\mathrm{b,int}}(t) \tag{16}$$

3.3 Signal Processing Model

As already described in the general architecture in Fig. 1 the synthetic signals from the Radar Signal Simulation have to be interpreted. For this task we developed a model-based signal processing chain similar to a regular automotive FMCW signal processing. In Fig. 5 the consecutive components are visualized. Within the model based signal processing each layer can directly be accessed. This is particularly helpful for the validation task. Beside the application in the simulation environment, the signal processing can also be used with real sensor measurements from the reference sensor. Based on the generic approach presented by [11], we developed an application specific variation for our model based signal processing in Fig. 5. First, the processing chain receives the down-converted antenna time signals. On that basis, modules for filtering and windowing are applied to provide the Fourier transformation (FT), similar to [11].

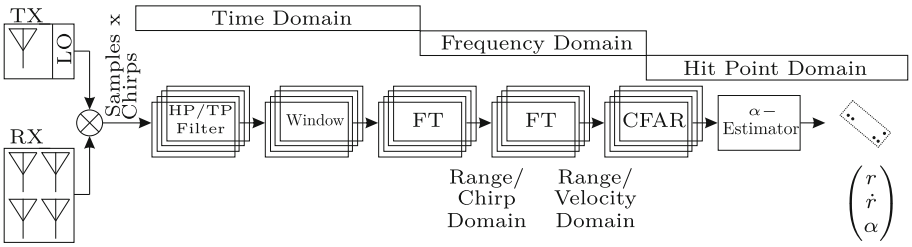

Fig. 5. Block diagram of the signal processing for simulated and measured radar echos.

After resolving in range-velocity domain, a Constant False Alarm Rate (CFAR) algorithm is applied, which is capable to detect targets as hit points in noisy environments [14]. For each detected cell in the RV-map, the phase differences over four receiving antennas will be used to estimate the azimuth angle, as described in [15]. Each hit point then consists of range r, velocity $\dot{r}$ and azimuth angle α.

4 Parametrization and Validation

For the validation of the radar and interference simulation we compared the model response with the real measurement behaviour on different processing

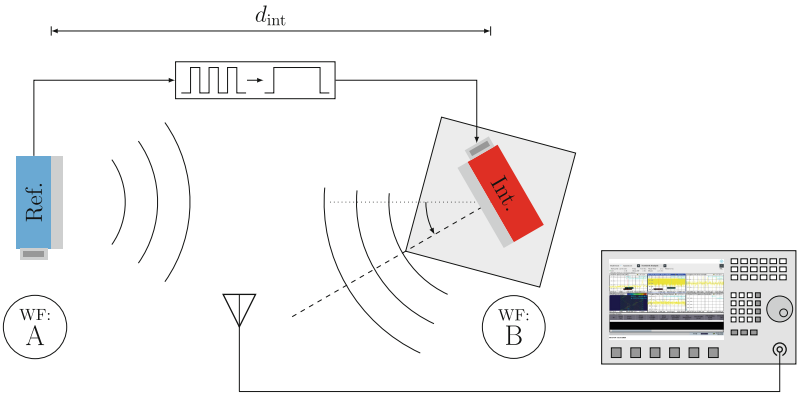

Fig. 6. General radar setup: modifications on the setup will be described in more detail.

Table 1. Parameters used for the measurement setup under asynchronous interference.

WF	Physical quantity	Symbol and unit	SI
A	Transmit power of vict. radar	$P_{\text{Tx,vict}} = 7$	[dBm]
	Start frequency	$f_{\text{start,vict}} = 76.2875$	[GHz]
	End frequency	$f_{\text{end,vict}} = 76.7125$	[GHz]
	Ramp duration	$T_{\text{c,vict}} = 25.6$	[µs]
	Chirp repetition time	$T_{\text{cc,vict}} = 42$	[µs]
	Antenna gain	$G_{\text{ant}} = 13$	[dBi]
	Rx pathloss	$L_{\text{Rx}} = 11.2$	[dB]
B	Transmit power of interferer	$P_{\text{Tx,int}} = 12$	[dBm]
	Start frequency	$f_{\text{start,int}} = 76.25$	[GHz]
	End frequency	$f_{\text{end,int}} = 76.675$	[GHz]
	Ramp duration	$T_{\text{c,int}} = 22.5$	[µs]
	Chirp repetition time	$T_{\text{cc,int}} = 38.8$	[µs]
	Antenna gain	$G_{\text{ant}} = 28.5$	[dBi]

layers. Based on the results, the model gets adapted and parametrized. The measurements were realized on the basis of a general radar setup illustrated in Fig. 6. It consists of two radar sensors with adaptable waveforms. The reference sensor is triggering the interference radar by the first chirp in a sequence. This guarantees a deterministic and reproducible interference impact for the measurements. The sensors are aligned straight to each other and the interferer is mounted on a rotating module. For interference verification a spectrum analyzer is triggered by the same signal to capture the wave superposition. The waveforms of both sensors (**WF:A** and **WF:B**) are described in the following Table 1.

Table 1 contains the chirp-frequencies, the transmit time and the power of both radars. The waveforms were applied with similar chirp slopes. This results in a low mixer frequency-deviation and yields in a good observability of the interfering effects. With the given setup the validation will be performed in the following. The main focus here is the correct estimation of the signal-powers in the RV-map which is crucial for detecting targets with and without interference.

4.1 Sampling Layer

On the sampling layer the filters get validated because they affect the Signal-to-Noise Ratio (SNR) of a reflecting target. The high- and low-pass filters in the radar front-end from Fig. 3 are implemented with the specified parameters from the datasheet. As the spectral components filtered by the high-pass filter correspond to very close objects, that do not occur in automotive scenarios, its performance is not validated as part of this work. Whereas for the low-pass filter we validate our assumptions as follows. The model is parametrized with a 7.5 MHz Butterworth low-pass-filter of order three and a Chebychev decimation filter. The latter is used to reduce the amount of data to be processed, as the ADC operates at 40 MSa/s while the information on frequencies above 20 MHz is not relevant for the sensor. For a better comparability during the validation, we approximate the interference signal's envelope with a clipped Gaussian. This method also features a technical analogy with the filter characteristics, as it approximates the frequency response of the filter. Knowing that the analyzed signal is a frequency sweep, it's envelope can be understood as it's frequency response. Figure 7 shows, that the envelopes of the simulated and measured signals match. We can expect that the simulated signal-power behind the filter induced by an interferer can be simulated sufficiently accurate.

Beside the filter-characteristic the noise also has an influence on the SNR of targets and therefore on their detectability. Typically radar front-ends, like the one depicted in Fig. 3, are System-on-Chip (SoC) solutions in which we expect to find active and passive components. In the literature, the noise of such devices

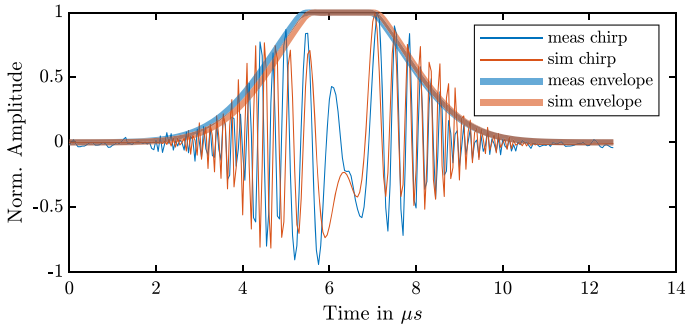

Fig. 7. Validating the low-pass filter by comparing the measured and simulated amplitude response and their envelope from an asynchronous-interfered receive signal.

are mainly described by thermal-noise, which has a constant spectral energy distribution [25]. Beside that, the 1/f-noise decreases with rising frequency. For the detection of targets in the spectrum, we know from Eq. 9 that the frequency is related to the distance of a target. Consequently, the frequency dependence of the noise can be interpreted as range dependent noise. In order to accommodate this effect in the simulation, the spectral density of the noise was measured with the reference sensor. Therefore, the initial measurement setup from Fig. 6 is modified, such that no power is being transmitted by both radar sensors. As the receivers are still operational, it is possible to capture the noise sources mentioned above. The measured spectral distribution (see red graph in Fig. 2) already contains the high- and low pass transfer functions. During simulation the generated noise is added to the signal before the radar front-end with its filters. Therefore it is necessary to undo the effect of the filters on the measurement (see blue graph in Fig. 8). In the simulation the noise is generated according to this data. This is done by generating complex white Gaussian noise in the frequency domain and multiplying it with the depicted transfer characteristic. A transformation into the time domain yields Gaussian noise, that is now correlated according to the sensors noise. This noise characteristic will be applied in the *Noise Time Signal* block from the model architecture in Fig. 2.

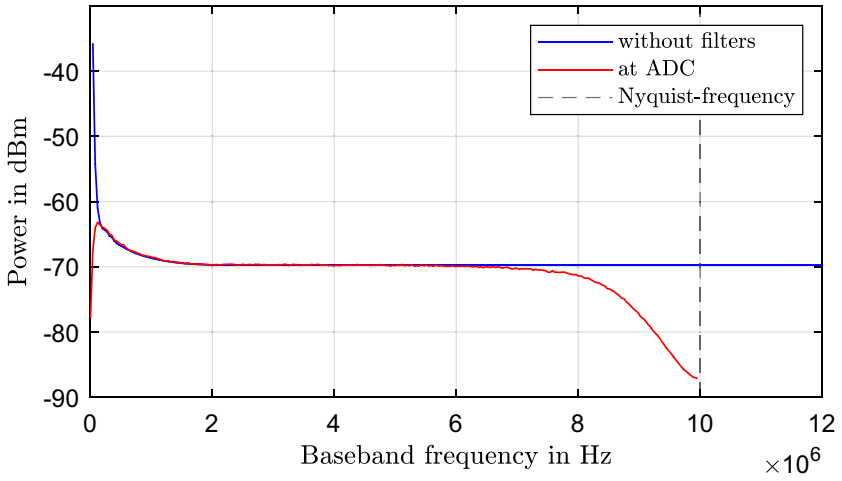

Fig. 8. Noise floor (blue) leads to spectral power density at the ADC (red). It is important to note that the power at the ADC was amplified by 45 dB as part of the analog radar front-end. (Color figure online)

Additionally the nonlinear behavior of the radar receiver path in Fig. 3 is modelled as a device with saturating properties. Based on the general measurement setup depicted in Fig. 6, we rotate the victim radar towards the interferer, which is configured to generate synchronous interference. During this rotation

the received signal level changes with the directivity of the antenna. With the given antenna pattern we calculate an expected signal-power for the case of a completely linear receiver. By comparing the measured saturating signal with the expected signal, we extract the saturation curve as depicted in Fig. 9. As radar sensors differ greatly in their operation under the exposure of high signal-powers, we ensure that the operating point of the simulated radar sensor lies within the linear region for all subsequent simulation and measurement sets.

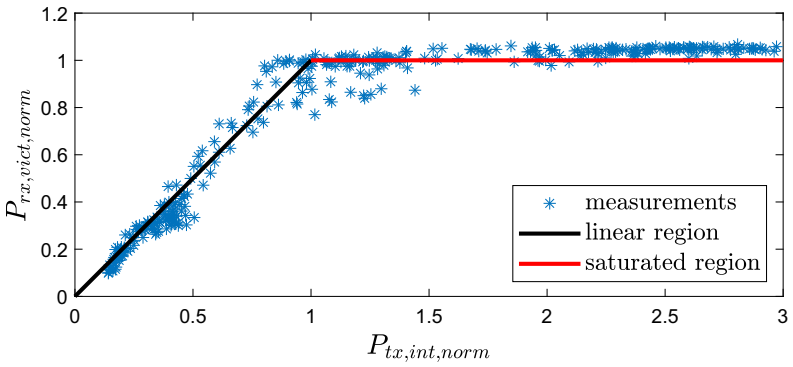

Fig. 9. Measurement analysis and linearization of the receiver path in the victim radar.

4.2 Signal Layer

On the signal-level, we validate the model's ability to reproduce the received signal-power. As a first step, the model was parametrized with the receiver amplifier gains according to the datasheet. As a validation step, we conducted a series of measurements and simulations of that same set-up. Finally, we compared the reflected signal-powers in the simulation and measurements. The target of interest is a corner reflector with the side-length of 12 cm. According to [23] these dimensions translate into an radar cross section (RCS) of 17.5 dBm^2. While this value was confirmed with a calibrated setup our non-calibrated reference sensor outputs 1.3 dBm^2. The deviation of 16.2 dB originates from PCB losses and the sensor specific gain. Based on additional measurements by the manufacturer, we decreased the transmitted signal-power by 5 dB to accommodate the PCB losses in the transmitter path. In the receiver path we reduced the amplification gain by 11.2 dB.

4.3 Hit Point Layer

Whether a hit point gets detected as such depends on the Signal-to-Noise Ratio (SNR). The signal level is unaffected by interference, while the interference components can often be interpreted as noise. Therefore, the increased

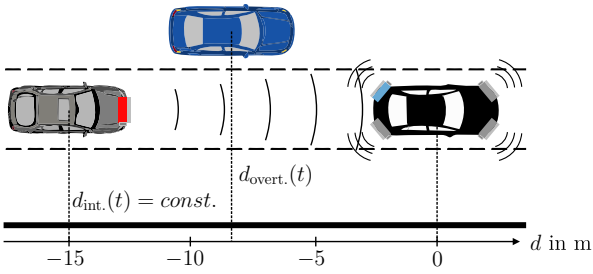

Fig. 10. The scenario describes an overtaking maneuver with an interferer in constant distance. For validation the hit points are measured over the distance $d_{\text{overt.}}$. (Color figure online)

noise level reduces the SNR, leading to a loss of hit points. The simulation should predict the number of lost hit points on extended objects. The reflectivity of each hit point depends on the orientation of the corresponding extended object. We parametrized the angle dependent RCS of a regular car with reference to [26]. For the evaluation, we took measurements of an approaching car (blue) with a constant relative velocity of $v_{\text{overt.}} = 10\,\frac{\text{km}}{\text{h}}$ as described in Fig. 10. The observed sensor (light blue) inside the ego vehicle (black) gets interfered by the front radar (red) mounted on the follower car (grey). In the simulation, we positioned a car at the same distance $d_{\text{overt.}}(t = 0)$ and recreated the trajectory relative to the ego vehicle. The post-processing was conducted on both datasets. An analysis of the hit points over the scenario yields a similar accumulation of the received signal-power. In Fig. 11 the power distributions for two exemplary $d_{\text{overt.}}$ are depicted. Especially for the low powered hit points which might be affected by interference, the distribution fits very well. The remaining deviation in the distribution of the received signal-power can be attributed to the fact that the RCS is parametrized for a different car. Beside that, the geometric scenario simulation has a lack of modelling details. For example, the rotating wheels and the car's

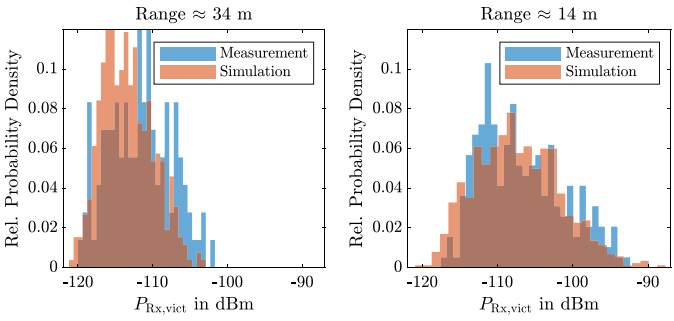

Fig. 11. Energy distribution from the hit points of a radially approaching car.

shape are not taken into account. At the same time, the distribution fits well enough to simulate the number of hit points getting lost at a varying noise level.

4.4 Scenario Layer

On the scenario layer the estimation of the overtakers' state (position and radial velocity along with other parameters) is particularly important. In the automotive application the objects' state is estimated with tracking algorithms, which consider information from the past. Instead of using tracking algorithms, which introduce complexity while obscuring the causality, we use a different measure. As all trackers rely on the availability of hit points, we compare the number of observed hit points along the scenario. The comparison in Fig. 12 shows the measurement and simulation results with and without the influence of interference.

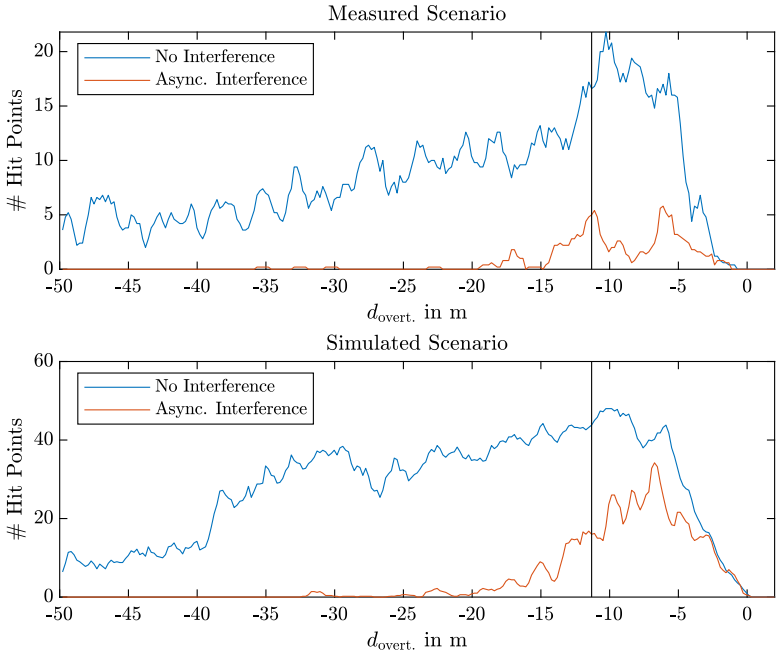

Fig. 12. Hit points from the overtaking car over $d_{\text{overt.}}$ in the simulation and the measurement. For a better comparability, the number of hit points were averaged over five time-steps. The vertical line indicates the boundary after which the data behind the vehicles RCS is no longer applicable in the simulation.

The graphs indicate that the number of hit points drop significantly with the activated interferer as expected. This result can be observed based on the measurement and simulation.

The quantitative analysis shows, that the simulation yields between up to four times as many hit points. This can be traced down to the fact, that the assumed hit points along the vehicle's contour do not accurately describe the surface details of a car. However the trend appears trustworthy, as well as the ratio of hit points with and without interference. Both, measurement and simulation indicate, that the overtaker can be reliably detected from a distance $|d_{\text{overt.}}|$ of greater than 50 m in the non-interfered case. Both methods similarly indicate that the distance of a reliable detection drops down to 20 m under the influence of the interferer.

The vertical line in Fig. 12 indicate the minimum distance at which the simulation follows the trend of the measurement. The derivation beyond this line can be explained by the assumption concerning the target illumination. The vehicle's RCS from [26] assumes planar waves, which is not valid in close distances.

5 Application Example

Based on the validation with real sensor measurements, the parametrized simulation can be used for testing interference mitigation methods. As an example we implemented and applied one state-of-the-art interference mitigation technique in the framework. First, the interference occurrence is detected by high signal amplitudes. Then, the method substitutes the interfered signal portions with zero [8]. For the test of this mitigation method in the simulation, we chose the overtaking scenario. Similar to previous measurements, the simulated car was approaching with a constant velocity towards the victim radar in the ego vehicle. The following Fig. 13 presents the number of measured hit points for the approaching car over a portion of discrete time steps in simulation. The analysis shows that the zero-algorithm is able to prevent most of the hit point loss from

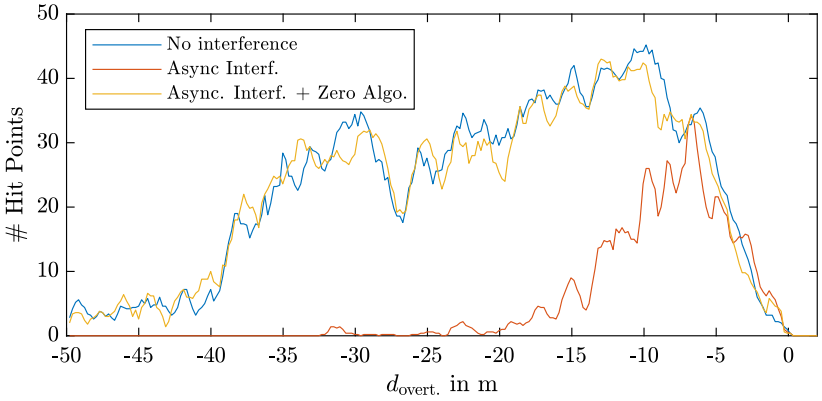

Fig. 13. Evaluation of the zero-algorithm based on the simulated hit points over $d_{\text{overt.}}$.

the target. Nevertheless, a main drawback of this mitigation method is the loss of the former time signal as stated in [9]. As a consequence, this might result in measurement inaccuracies on hit point data level. The simulation framework supports all investigations ranging from the development of such methods to the evaluation with scenario-based metrics.

6 Conclusion

In this research paper, we proposed a Radar Time Signal and Interference simulation for the development and test of interference mitigation techniques. We analyzed and validated all relevant artifacts, that are combined in the interfered target echo signal. We also considered the transmitter and receiver path of the radar front-end and their frequency response. The model was adapted in order to match the analyzed test setup. After model completion, we used our model to generate typical signal energy levels for the observed target and interference sources of a particular scenario. On the underlying sampling and signal layer we ensured that model inaccuracies can be quantified and related to their origin. Especially the power from the simulated hit points with and without interference was proven to be similarly distributed as measured. In the application, we used our simulation to a test state-of-the-art mitigation technique under particular interference scenarios. The resulting radar performance showed that the mitigation technique requires further examination and that the simulation is helpful for that purpose. Our future research will focus on a larger variety of testing scenarios and interference evaluation metrics. With the help of this, mitigation methods can be fully compared in the simulation framework.

References

1. Hummel, T., Kühn, M., Bende, J., Lang A.: Fahrerassistenzsysteme - Ermittlung des Sicherheitspotenzials auf Basis des Schadengeschehes der Deutschen Versicherer. GDV Forschungsbericht FS 03, (2011)
2. European New Car Assessment Programme: Test protocol - AEB VRU systems - Version 2.0.2. EuroNCAP (November 2017)
3. German Association of the Automotive Industry (VDA): Automation - from driver assistance systems to automated driving (2015)
4. ETSI EN 302 264: European Standard. https://www.etsi.org. Accessed 8 May 2020
5. Patole, S.M., Torlak, M., Wang, D., Ali, M.: Automotive radars: a review of signal processing techniques. IEEE Signal Process. Mag. **34**, 22–35 (2017)
6. Bordoux, A., Parashar, K., Bauduin, M.: Phenomenology of mutual interference of FMCW and PMCW automotive radars. In: 2017 IEEE Radar Conference (RadarConf), pp. 1709–1714 (2017)
7. Prinz, A., Roth, J., Schwendner, J., Ayeb, M., Brabetz, L.: Validation strategy for radar-based assistance systems under the influence of interference. In: 2020 German Microwave Conference (GeMiC), pp. 252–255 (2020)
8. Brooker, G.M.: Mutual interference of millimeter-wave radar systems. IEEE Trans. Electromagn. Compat. **49**, 170–181 (2007)

9. Bechter, J., Waldschmidt, C.: Automotive radar interference mitigation by reconstruction and cancellation of interference component. In: 2015 IEEE MTT-S International Conference on Microwaves for Intelligent Mobility (ICMIM) (2015)
10. Bechter, J., Roos, F., Rahman, M., Waldschmidt, C.: Automotive radar interference mitigation using a sparse sampling approach. In: 2017 European Radar Conference (EURAD) (2017)
11. Schipper, T., Schlichenmaier, J., Ahbe, D., Mahler, T., Kowalewski, J., Zwick, T.: A simulator for multi-user automotive radar scenarios. In: IEEE MTT-S International Conference on Microwaves for Intelligent Mobility (ICMIM) (2015)
12. Beise, H., Stifter, T., Schröder, U.: Virtual interference study for FMCW and PMCW radar. In: 2018 German Microwave Conference (GeMiC) (2018)
13. Holder, M., Linnhoff, C., Rosenberger, P., Winner, H.: The Fourier tracing approach for modeling automotive radar sensors. In: 20th International Radar Symposium (IRS) (2019)
14. Kronauge, M., Rohling, H.: Fast two-dimensional CFAR procedure. IEEE Trans. Aerosp. Electron. Syst. **49**, 1817–1823 (2013)
15. Iovescu, C., Rao, S.: The fundamentals of millimeter wave sensors. Texas Instrum. **SPYY005**, 1–8 (2017)
16. Hischke, M.: Collision warning radar interference. In: Proceedings of the Intelligent Vehicles 1995 Symposium (1995)
17. Goppelt, M., Bloecher, H.-L.: Automotive radar-investigation of mutual interference mechanism. In: Advances in Radio Science, pp. 55–60 (2010)
18. Kim, J., Lee, S., Kim, S.: Modulation type classification of interference signals in automotive radar systems. IET Radar Sonar Navig. **13**, 944–952 (2019)
19. Goppelt, M., Blöcher, H.-L., Menzel, W.: Analytical investigation of mutual interference between automotive FMCW radar sensors. In: 2011 German Microwave Conference (GeMiC) (2011)
20. Khoury, J., Ramanathan, R., McCloskey, D., Smith R., Campbell, T.: RadarMAC: mitigating radar interference in self-driving cars. In: 13th Annual IEEE International Conference on Sensing, Communication, and Networking (SECON) (2016)
21. Eder, T., Prinz, A., Brabetz, L., Biebl, E.: Szenarienbasierte Validierung eines hybriden Radarmodells für Test und Absicherung automatisierter Fahrfunktionen. In: Tille, T. (ed.) Automobil-Sensorik 3, pp. 21–43. Springer, Heidelberg (2020). https://doi.org/10.1007/978-3-662-61260-6_1
22. Gardill, M., Schwendner, J., Fuchs, J.: In-situ time-frequency analysis of the 77GHz bands using a commercial chirp-sequence automotive FMCW radar sensor. In: IMS - Recent Advances in Radar Systems Applications (2019)
23. Klausing, H., Holpp, W.: Radar mit realer und synthetischer Apertur - Konzeption und Realisierung. De Gruyter, Berlin (1999)
24. Skolnik, M.I.: Radar Handbook, 2nd edn. McGraw-Hill Inc., New York (1990)
25. Müller, R.: Halbleiter-Elektronik 15. Rauschen, 2nd edn. Springer, Heidelberg (1990). https://doi.org/10.1007/978-3-642-96960-7
26. Kamel, E.B., Peden, A., Pajusco, P.: RCS modeling and measurements for automotive radar applications in the W band. In: 11th European Conference on Antennas and Propagation (EUCAP) (2017)